Local Mechanism of Phenyl Ring π-Flips in Glassy Polycarbonate

Duane R. Whitney and Robert Yaris*

Department of Chemistry, Washington University, St. Louis, Missouri 63130

Received July 30, 1996; Revised Manuscript Received November 15, 1996[⊗]

ABSTRACT: In order to obtain the mechanism for the infrequent phenyl ring π-flips in glassy polycarbonate, a generalized Langevin dynamics simulation was performed on a reduced model consisting of a flipping ring and its keeper ring. The frequency of π-flips and activation energy for π-flips obtained from the simulation are in agreement with experiment. A phenyl ring π-flip occurs when there is an increase in the separation distance between the ring and its nearest neighbor ring on another chain, accompanied by, and in synchrony with, an increase in its rotational kinetic energy.

I. Introduction

The phenyl rings in glassy polycarbonate have been shown by solid state NMR[1] to undergo rapid but infrequent π-flips with a time scale[2] O (10^{-5} s). Since the phenyl rings of polycarbonate in solution are free rotors,[3] on the NMR time scale, the infrequent π-flips in the solid must be caused by the interactions between the ring and its neighboring chains in the glass. That is, there must be a density fluctuation in the solid to give the ring "enough room" to rotate. This density fluctuation then closes down, trapping the ring after it has been rotated by π; *i.e.*, it has performed a π-flip. Thus the phenyl ring π-flips can be viewed as reporting on density fluctuations in the glass. Since phenyl ring π-flips have been shown[4] to be related to the low-temperature (−120 °C) peak in the dynamic mechanic loss spectrum of polycarbonate, it is clear that an understanding of the π-flips is essential in order to understand the properties of polycarbonate.

Some time ago, we presented[5] an intuitive mechanism for the π-flips which could qualitatively explain the observation of infrequent π-flips. However, since the mechanism was made up "out of whole cloth", there was no compelling reason to believe it. We also simulated[6] a two-dimensional array of benzene rings which qualitatively agreed with the above-mentioned π-flip mechanism. However, glassy polycarbonate is not a two-dimensional array of benzene rings. In this paper, we shall simulate the π-flips, thus obtaining the mechanism from the simulation.

The idea of simulating the motion of infrequent events on the time scale of the π-flips in polycarbonate raises an immediate problem—it cannot be done in the standard way using molecular dynamics. The reason for this is that the very strength of molecular dynamics, its conceptual simplicity (one is just solving Newton's equation on a computer), is also its weakness. The time scale for a molecular dynamics simulation is set by the fastest motion in the problem. That is, in the numerical solution of the differential equation, one must discretize the time scale and the time step must be short compared to the motion which one is trying to simulate. Hence, since *real* computers have a finite speed, there are limits on what can be simulated. In the case of π-flips in polycarbonate, we estimate that it would take O (10^4 years) on a dedicated supercomputer to see a single π-flip. Clearly, a "brute force" molecular dynamics simulation of the π-flips is out of the question.

Since the time scale of the simulation is set by the problem, and waiting around for a fast enough computer is clearly the coward's way out (and probably would not happen in our scientific lifetime), we have recently developed[7] a computational method which allows one to simulate infrequent events. This method, called generalized Langevin dynamics (GLD), is briefly reviewed in section II. However, the truly interested reader is urged to read the original papers[7] and references therein.

The GLD method requires as input a standard molecular dynamics simulation performed for a relatively short time. This brings up the second major problem with performing a molecular dynamics simulation of polycarbonate—one cannot, with present day technology, simulate an amorphous polymer glass. What allows us to proceed is the fact that the phenyl ring π-flip is a local problem. Any given phenyl ring is constrained from rotating by its neighboring chains. Thus we need only simulate a small volume of the solid. To this end in section III we extend the model for local chain packing which Klug *et al.*[8] (to be referred to as the KZTS model) obtained by melding experimental average interchain atomic distances measured by solid state NMR methods with the X-ray structure[9] obtained for a crystalline dicarbonate model for polycarbonate, [4,4-isopropylidenediphenylbis(phenylcarbonate)]. This will be accomplished by doing a simulation (referred to as the full simulation) of the KZTS model, using some of the experimental interchain distances as distance constraints by means of additional constraining potentials, obtaining a thermalized, relaxed version of the KZTS model of local chain packing in glassy polycarbonate. As will be shown, when the KZTS model thermally relaxes, it distorts, somewhat reminiscent of a Peierls distortion,[10] into a layered lattice with alternating long and short interchain distances.

An implicit assumption in the present work is that a glassy polymer has a short range local order but not a long range order. In this respect the glass is like a liquid, which also has short range but not long range order. In fact the glass can be considered as a kinetically frozen liquid. We have previously shown,[11] using a Monte Carlo simulation, that polymer chains in the melt have a local preference for ordering parallel as long as they have some chain stiffness. Explicitly, the polycarbonate chains in the glass locally pack as bundles of parallel chains. This picture of disordered bundles

[⊗] Abstract published in *Advance ACS Abstracts,* February 1, 1997.

S0024-9297(96)01143-6 CCC: $14.00

of locally parallel chains is in accord with the surface irregularities observed by atomic force microscopy by Kowalewski and Schaefer.[12] Since the full simulation is a lattice simulation it probably somewhat overemphasizes the local order. However, we feel that within the constraints of what is technologically feasible it contains enough of the local (but not global) physics to enable us to go on to the reduced GLD simulation in section IV. The results of the simulation will be given in section V, to be followed in section VI by a discussion which will include the implications of this study for understanding the unusual toughness properties of polycarbonate.

The only other calculation[13] (of which we are aware) of phenyl ring π-flips in glassy polycarbonate, which is more than a single chain calculation, by Hutnik *et al.* is a static energy minimization calculation. They start out from their rather amorphous energy-minimized structure of polycarbonate[14] and rotate a phenyl ring, reminimizing the energy as they rotate. While they do obtain a reasonable activation energy (see section V, below), as is pointed out by KZTS their structure is not in agreement with the measured distances in polycarbonate and they do not get the experimental density correct. We think that this is caused by there not being enough local order in their structure.

II. Generalized Langevin Dynamics

A. Equation of Motion. The way we are able to simulate a physical process over a long period of time is to drastically reduce the number of degrees of freedom of the problem, retaining only those degrees of freedom in which we are interested. Such a drastic reduction allows for a massive increase in the length of physical time over which one can follow the "interesting" degrees of freedom on the computer. We are interested in the physical mechanism for the phenyl ring π-flips in glassy polycarbonate, so we will retain the phenyl ring of interest and the parts of the neighboring chain(s) with which the ring is strongly interacting. An explicit description of the retained degrees of freedom is deferred until section IV. It should be emphasized, however, that the decision on which degrees of freedom are retained and which are suppressed constitutes a model for the physical system of interest. The construction of such a model requires the modeler to use physical intuition about the system and also perhaps some computational experimentation. In the real world, this frequently requires a compromise between what one would like to include and the necessary reduction which allows the problem to be done.

Of course the retained degrees of freedom (motions of the phenyl ring and its near neighbors) are not in isolation. They are interacting with all of the other parts of the system which we want to suppress. Hence, if we want a model of the interesting part of the system which, when simulated on the computer, faithfully reproduces the behavior that the subsystem of interest would exhibit in the whole system, we must include the effects of these interactions with the suppressed degrees of freedom on the retained subsystem. That is, we must have an equation of motion which includes the effects of the suppressed degrees of freedom on the explicitly expressed degrees of freedom. The interaction (forces, potentials) with the suppressed degrees of freedom must, in principle, be time dependent. The origin of this time dependence is that the retained subsystem is not an energy conserving system. It is constantly exchanging energy with the suppressed degrees of freedom. Time independent interactions result in energy conservation—hence the interaction must be time dependent.

Historically, the first such equation of motion was produced by Langevin[15] to describe the motion of a diffusing solute molecule with all of the solvent degrees of freedom suppressed. The Langevin equation is

$$m_i\dot{\mathbf{v}}_i(t) = \mathbf{F}_i(t) + \xi_i\mathbf{v}_i(t) + \mathbf{R}_i(t) \tag{1}$$

where m_i is the mass of solute particle i, $\mathbf{v}_i$ is its velocity, $\mathbf{F}_i(t)$ is the sum of any other forces on particle i, ξ_i is the frictional coefficient, and $\mathbf{R}_i(t)$ is a normally distributed random force such that

$$\langle\mathbf{R}_i(t)\rangle = 0 \tag{2}$$

where the angular brackets denote an equilibrium average. This is just Newton's equation for a particle in solution with effects of the suppressed solvent degrees of freedom on the solute particles provided by a frictional term (a dissipative force) and a random force (an impulsive force). Since a solute must come into equilibrium with the solvent, in the long time limit, independent of the initial conditions of the solute particles, the impulsive random force and the dissipative frictional force must approach a balance. This balancing of the forces leads to the fluctuation dissipation theorem

$$\langle\mathbf{R}_i(t)\,\mathbf{R}_j(t')\rangle = 2m_ik_B\xi_iT\delta(t-t')\delta_{ij} \tag{3}$$

where k_B is Boltzmann's constant, T is the temperature, $\delta(t-t')$ is a Dirac δ function, δ_{ij} is a Kronecker delta and $\langle\mathbf{R}_i(t)\,\mathbf{R}_j(t')\rangle$ is the random force autocorrelation function.

The Langevin equation can be used as the equation of motion in a molecular dynamics simulation instead of Newton's equation. Such a simulation, called Brownian or Langevin dynamics, is standardly used for molecules in solution to incorporate the effects of the solvent without explicitly including the solvent degrees of freedom into the simulation.

The Langevin equation includes the effects of the suppressed degrees of freedom on the retained degrees of freedom in an averaged mean field fashion. However, it does not account for the back-interaction where the retained degrees of freedom alter the suppressed degrees of freedom which in turn interacts back on the retained degrees of freedom. This can be rigorously formulated into a generalized Langevin equation[16]

$$m_i\dot{\mathbf{v}}_i(t) = \mathbf{F}_i(t) - m_i\int_0^t\mathrm{d}t'\,\phi_i(t')\,\mathbf{v}_i(t-t') + \mathbf{R}_i(t) \tag{4}$$

where $\phi(t)$ is the time dependent memory function which includes all these many-body effects. Here the additional force term includes the interactions between the retained degrees of freedom. In addition, the force term frequently must include effective time independent forces when some of the interactions with the suppressed degrees of freedom served to limit the motions of the retained degrees of freedom. For example, if one is looking at a particle in a solid, the interaction of the particle with its neighbors serves to restrict the motion of the particle to the neighborhood of its equilibrium position (at least for a long time). If some of the neighboring particles are no longer explicitly included in the calculation, their restraining effect must be included in the equation of motion via an effective force. These time independent effective forces can in principle

be included as time independent parts of the memory function, but it is much more convenient to separate out the time independent parts. Hence the memory functions contain the information about the effects of the fast modes of the suppressed degrees of freedom on the retained subsystem while the effective potentials model the static effects of the deleted part of the lattice as well as slow modes.

Again, in the long time limit, the retained degrees of freedom must be in equilibrium with the suppressed degrees of freedom and the balance between the random force and the memory function are assured by the fluctuation dissipation theorem

$$\langle \mathbf{R}_i(t)\, \mathbf{R}_j(t') \rangle = 2 m_i k_B T \phi_i(t-t') \delta_{ij} \tag{5}$$

The memory function has the form of a self-interaction. That is, the retained degrees of freedom interact with themselves at an earlier time. They have a memory of their previous states. This feature of a self-interaction is a quite general feature of many-body theories where some of the degrees of freedom are suppressed. For example, in the field theoretic formulation of many-body quantum mechanics,[17] the kernels of the integral equation for reduced Green's functions contain a self-energy (or more generally a vertex function) of this form. If the memory function is approximated as time independent, *i.e.*, no self-interaction, one recovers the Langevin equation, eq 1, as the mean field approximation to the generalized Langevin equation, eq 4.

This reduced equation of motion, the generalized Langevin equation, can now serve as an equation of motion for a simulation of the retained degrees of freedom in the presence of the suppressed degrees of freedom —a generalized Langevin dynamics simulation.

B. Simulation Method. The first problem that arises in attempting to use the generalized Langevin equation as an equation of motion is that one must know the memory function. Since the memory function embodies the many-body effects which include the suppressed degrees of freedom, it clearly must be approximated. The standard approach in many-body theories[17] is to approximate the self-interaction using some form of perturbation truncation. Unfortunately, this will not do here, since we do not have a good model for the zeroth-order dynamics about which we could expand in a perturbation series. In fact, if we had such a good zeroth-order model, we would not be doing this problem. It is just this zeroth-order model of the phenyl-ring π-flips which is the goal of this paper. What saves us and allows us to use the generalized Langevin equation as an equation of motion is that memory functions must decay quickly in time. The physical reason for this rapid decay of the memory function is that the memory is a result of a nonequilibrium perturbed state of the suppressed degrees of freedom. Such nonequilibrium states quickly thermalize, decaying to their equilibrium, *i.e.* averaged, state in just a few "collisions". Thus, the self-interaction or memory can last only for the short time until the "perturbed state" has decayed away.

Since the memory function is short lived, it can be fit to the results of a full simulation of the system with no suppressed degrees of freedom. This is possible since the full simulation does not have to be carried through for a long time. That is, we first guess a form for the memory function(s), with some adjustable parameters which are to be fit to the full simulation. The form chosen is always a compromise between ease of computation and the desire for enough flexibility to model adequately the problem. This choice usually requires some computational experimentation. In the work presented here, we used exponentials for all memory functions.

The second problem which arises once one has the functional form(s) of the memory function(s) is what properties of the full simulation should one use to fit the adjustable parameters. Our procedure here has been to use correlation functions which most closely resemble the degrees of freedom in which we are interested. For example, in fitting the memory function for the phenyl ring angular motion, we use the ring angular autocorrelation function $\langle \theta(t)\, \theta(0) \rangle$, where θ(t) is the angle about the ring C_2 axis at time t. We fit the effective potentials in a similar way. For example, in fitting the potential for the center of mass motion of the ring, we use the distribution function for the ring motion as well as the distance autocorrelation function where the distance involved is the distance to a nearest neighbor on another chain. In all of these cases, some intuition and some computational experimentation are required in order to select the relevant correlation functions and distribution functions.

The procedure then is to adjust the parameters until the results obtained from the reduced generalized Langevin dynamics simulation are in agreement with the results obtained from the full simulation within the errors of the simulation. In actuality, this is an iterative and somewhat tedious procedure since adjusting a parameter to correct one distribution function can cause another one to deviate from the full simulation. The major reason for this is that the degrees of freedom we are looking at are not normal modes (which would be global modes of the system) but rather are local motions of the system. Hence the retained degrees of freedom are strongly coupled together. In addition, the partitioning between the effective potentials is not unique. Again, this is partly due to the degrees of freedom not being normal modes. After all, each particle sees only the total force on it, not how it has been partitioned for our convenience.

The third (and last) major problem in using the generalized Langevin equation as an equation of motion for a simulation is to enforce the fluctuation dissipation theory, eq 5. We do this by treating the random force as a second-order Markoff process. That is, we find a string of random forces $\{R_n\}$ such that

$$R_{n+1} = \phi(\Delta t) R_n + 2 m k_B T W_n \tag{6}$$

where Δt is the length of our discretized time step, *i.e.*,

$$t_{n+1} = t_n + \Delta t \tag{7}$$

$\phi(\Delta t)$ is the memory function evaluated at time Δt, *i.e.*, after the first time step, and W_n is a normally distributed random number with zero mean. In general, eq 6 is an approximation to the fluctuation dissipation theorem, eq 5, since it is the lowest order version of an autoregressive algorithm.[18] However, it can be shown that for exponential memory functions

$$\phi_i(t) = \alpha_i e^{-\gamma t} \tag{8}$$

the second-order Markoff process, eq 6 is the correct solution to the fluctuation dissipation equation, eq 5. In the present treatment the index i in eq 8 will refer

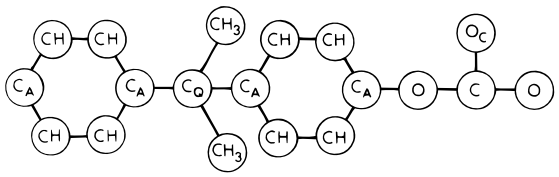

Figure 1. Monomer repeat unit.

to the coordinates θ, x, y, or z. The string of random forces $\{R_i\}$ calculated by eq 6 is then used in the numerical solution of the generalized Langevin equation.

As discussed above and elsewhere,[7,16] the GLD simulation is a theoretically justified method to reproduce the results of a full simulation, if only we could do the full simulation. It also has an experimental justification. In our previous papers[7] we showed that for the case of a simplified model system, a two-dimensional array of interacting benzene rings, where the full simulation could be performed long enough to see the benzene rings π-flip, the GLD simulation reproduced both the frequency and mechanism obtained by the full simulation. The fact that the GLD method has a theoretical foundation and has worked in the past to reproduce known results for a simplified, but not unrelated, model is our justification for using this approach for the more realistic situation where we cannot obtain the π-flip mechanism by a full simulation.

III. Full Simulation

A. Initial Conditions. A lattice model to depict the local structure of polycarbonate was generated from the monomer repeat unit depicted in Figure 1. Starting with the KZTS schematic model a six monomer long chain forms the backbone of each polycarbonate fragment. The lattice was then constructed using 49 such chains leading to a $6 \times 7 \times 7$ lattice. The lattice distances are the result of imposing the KZTS experimental distance constraints within horizontal and vertical planes, and by imposing a density constraint. The values of the distance parameter and the experimental constraint distances are listed in the first column of Table A8 of Appendix A. Within each horizontal plane the fragments are equally spaced due to the 6.0 Å carbonyl−carbonyl distance constraint. Vertically, the distances between the planes alternate. This spacing is determined by a carbonyl carbon−quaternary carbon distance constraint and a carbonyl carbon−methyl distance constraint. The spacings differ because there are two distinct types of chains in each vertical slice; *i.e.* alternate chains are inverted. See KZTS Figure 8b. The ternary carbon atoms are perpendicularly aligned in the vertical layers, and the carbonyl groups are aligned perpendicularly in the horizontal layers.

In order to obtain a lattice, the KZTS model was adjusted by straightening the backbone by placing the ternary carbons horizontally in-line. Also, since benzene rings tend to pack in a nearly perpendicular minimum energy configuration, the phenyl rings along the backbone and between nearest neighbors were rotated about their C_2 axis to obtain perpendicularity. The resulting spacing lattice is shown in the left panel of Figure 2. In the simulation, the outer monomer units in the lattice are held fixed so that out of the $6 \times 7 \times 7$ lattice only the central $4 \times 5 \times 5$ sublattice is mobile. However, only the central monomer and its nearest neighbors will be used in all results, in order to minimize edge effects.

B. Potential. The potential function and the parameters were based on the united atom CHARMM[19] potential. All atoms, except for hydrogens, are treated as single particles. Hydrogen atoms are subsumed in the potential for the carbon atoms they are attached to, *e.g.*, methyl groups and aromatic CH's are treated as single particles (see Appendix A, Table A1). The functional forms of the potentials are

$$\text{bonding atoms:} \qquad V = \frac{k_b}{2}(s - s_0)^2 \tag{9}$$

$$\text{bond angle:} \qquad V = \frac{k_\theta}{2}(\theta - \theta_0)^2 \tag{10}$$

$$\text{torsion angle:} \qquad V = k_\phi[1 + \cos(n\phi)] \tag{11}$$

$$\text{improper torsion:} \qquad V = \frac{k_i\phi}{2}(\phi - \phi_0)^2 \tag{12}$$

$$\text{Lennard-Jones:} \qquad V = 4\epsilon\left[\left(\frac{\sigma}{r}\right)^{12} - \left(\frac{\sigma}{r}\right)^{6}\right] \tag{13}$$

where s is the bond length, θ is the bond angle, ϕ is the torsional angle, n is an integer, σ is the Lennard-Jones radius, and ϵ is the Lennard-Jones well depth. The potential parameters are listed in tables in Appendix A, Tables A2−A7.

Following Hutnik *et al.*[20] we replaced the torsional potential for rotation about the axis of the aromatic ring by

$$V = \frac{k_r}{2}(1 + \cos\{4[\phi - 0.3\sin(2\phi)]\}) \tag{14}$$

in order to produce the correct energy minimum. We did not include any electrostatic interactions.

Intramolecular Lennard-Jones interactions between nonbonded atoms were included for those atomic pairs separated by four or more bonds. The Lennard-Jones parameters were adjusted to reproduce the experimental result for polycarbonate in solution, where the phenyl rings appear as free rotors on the NMR time scale.[3] Scaling the Lennard-Jones radii by 0.89 yielded an estimated intramolecular barrier to phenyl ring rotation of less than 2 k_BT. This was checked by performing a single chain Brownian dynamics simulation which showed that the resulting time between phenyl ring rotations was too short to be observable by NMR. Hence all intra-chain Lennard-Jones's were scaled by 0.89 from the values given in Table A5.

The experimental distance constraints were maintained by imposing additional harmonic constraining potentials

$$V = \frac{k_s}{2}(s - s_0)^2 \tag{15}$$

where s_0 is the experimental distance determined by KZTS and the force constant was adjusted so that the (mean square) spread in the constrained distance was consistent with the experimental uncertainty. These parameters are listed in Table A8.

C. Simulation. The simulation was performed using Brownian (Langevin) dynamics with a fictitious frictional constant.[21] That is, the time trajectory of each particle in the system is generated by a Langevin equation of motion, eq 1. The fictitious frictional

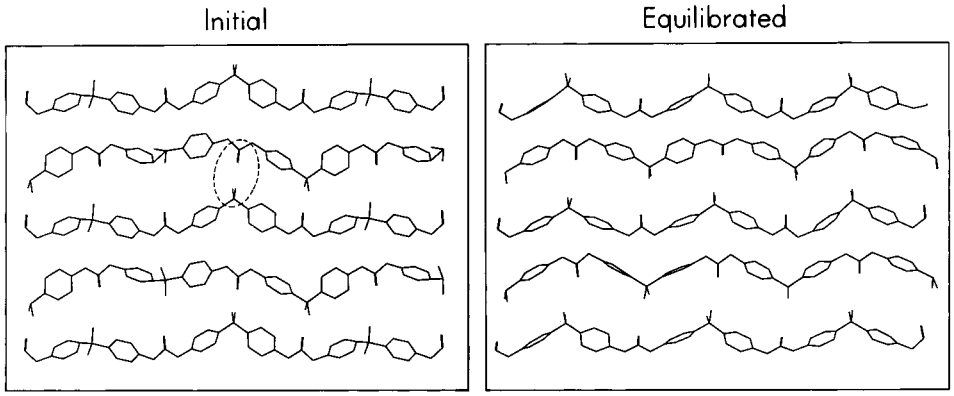

Figure 2. Chain packing. The left hand panel is a vertical slice through the lattice, showing the starting structure for the simulation. Only the mobile part of the lattice is shown (see text). The dotted lines show the region of two of the nearest neighbor constraint distances [carbonyl C−quaternary C and carbonyl C−methyl C]. The third constraint distance [carbonyl C−carbonyl C] cannot be shown in this perspective. The right hand panel shows a snapshot of the same vertical slice for a fully equilibrated lattice.

constant, as well as the corresponding random force that is autocorrelated to it via a fluctuation dissipation theorem, allows for an interaction with a fictitious heat bath. The purpose of the fictitious heat bath is to maintain the system at the desired temperature without the necessity of periodically rescaling the kinetic energy. The simulation parameters are listed in Table A9.

The time trajectories were generated using the Verlet finite difference algorithm.[22] As mentioned above, the outer monomers along the boundary of the lattice are stationary for all simulations. During the initial equilibrium all quaternary carbons were fixed in order to straighten the lattice. The entire inner lattice was then relaxed at a low temperature using small time steps for several picoseconds. The lattice was then equilibrated at room temperature (300 K) for 10 ps. We then obtained a 100 ps trajectory which was sampled at 5 fs intervals.

A Lennard-Jones interaction list and a 9 Å cutoff radius was used on all Lennard-Jones interactions. The interaction list (all interactions within the cutoff plus a 0.5 Å shell) was automatically updated during the simulation[22] when any one of the atoms within the whole lattice had moved 0.2 Å from the previous update, which occurred on average after 10−20 iterations.

D. Structural Results. As shown in the left panel of Figure 2, the starting conditions for the simulation had equally spaced lattice distances between the rings. However, almost immediately upon starting the simulation, the lattice distorted to give a layered lattice with alternating long and short distances between the chains, illustrated by a typical snapshot in the right panel of Figure 2. This layering took place within 1−2 ps during the initial pre-equilibration phase of the simulation, and this alternating layered structured remained stable throughout the simulation.

Since we were surprised at this result (and in fact did not initially believe it), we tried very hard to make it go away. We varied the potential parameters to try to eliminate the alternation by doing more than 50 different variations of the potential parameters with no effect. We then tried to change the lattice spacing but to no avail. We tried constraining the distances between only alternate layers with the same results. In fact since the results were the same whether we constrained every layer or alternate layers, in the effort to minimize the number of constraints, we did the final simulation constraining only alternate layers. That is, we constrained the carbonyl carbon−methyl distances for pairs of chains where the methyl pointed toward the carbonyl but not for pairs of chains where the methyl pointed away from the carbonyl; see Figure 2. We also only constrained the carbonyl carbon−quaternary carbon distances between the same pairs of chains.

Thus, since the layering effect is independent of the choice of potential parameters (as long as we keep them within reasonable bounds) and also of both the initial conditions and constraint conditions, we can only conclude that the layering is real. Moreover, the distance alternation agrees with the KZTS model in that each of the distances measured was to a single nearest neighbor.[8] The snapshot of the structure given in the right panel of Figure 2 is fully equilibrated using the potential parameters listed in Appendix A. Due to this alternation of distances, a ring is 2 Å closer to its nearest neighbor ring than it is to its next-nearest neighbor.

A second structural feature to emerge from the simulation was the angular orientation of the phenyl rings. The initial condition was for nearest neighbor rings to be perpendicular.[23] After equilibration, the rings remain essentially perpendicular along the backbone of a single chain but are parallel between layers. This is depicted in the snapshot, Figure 2. Again the change in ring angle was qualitatively independent of the choice of potential parameters.

Lastly, the registration between chains is shifted between horizontal layers.

E. Additional Results. As a check that the interchain potentials were scaled properly, we performed the simulation not only at the experimental density for an ordered bundle or region of (1.3 g/cm^3—the density of crystalline polycarbonate regions[24]) but also at a slightly lower density (1.25 g/cm^3) and slightly higher density (1.35 g/cm^3). At low density, the ring angle oscillations were much too large compared to experiments,[25] even with very large constraining potentials. At high density, the magnitude of the ring oscillations were reasonable, but the backbone of the chains became unphysically distorted during the initial equilibration. At a density of 1.3 g/cm^3, the mean square ring oscillations were consistent with the experimental NMR results, and the chains did not distort significantly. All of the reported results are for the final simulation done at a density of 1.3 g/cm^3.

The constraint potentials were adjusted to reproduce the experimental ring angle oscillations and constraint distances. The experimental distances used as constraint distances are given in the first column of Table

A8. The average values of those distances obtained from the simulation are given in the third column of Table A8. In comparing these two sets of numbers, one should keep in mind that the NMR experiment measures a distance as the inverse cube of the distance. Hence it is really very sensitive to the short distance. Or said another way, the average value of the distance obtained by averaging $(4.51\ \text{Å})^{-3}$ and $(6.14\ \text{Å})^{-3}$ is 4.78 Å.

As an independent check, we have three additional distances which were measured by NMR[26] and were not used as constraints in the simulation. The first is the distance from a ring carbon (ortho to the oxygen) to a deuterium on a phenyl ring in the nearest neighbor chain. The second distance is from the same ring carbon (ortho to the oxygen) to a methyl deuterium on the nearest neighbor chain. The third distance is from the carbonyl carbon to a methyl deuterium on the nearest neighbor chain. The experimental distances along with the average values of these distances obtained from the simulation are given in Table 1. As can be seen, the simulation reproduces the measured distances.

Table 1. Experimental and Simulated Unconstrained Intermolecular Distances for Bulk Polycarbonate

	measured (Å)[a]	simulated (Å)[b]
ring C−ring D	2.6 ± 0.4	3.0 ± 0.3
ring C−methyl D	3.2 ± 0.4	3.1 ± 0.3
carbonyl C−methyl D	3.8 ± 0.4	3.4 ± 0.13

[a] Reference 26. [b] The eror listed for the simulation is the half-width at half-maximum of the distance distribution function.

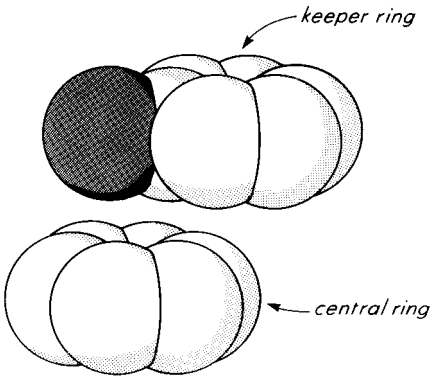

Figure 3. Reduced model. The upper ring is the "keeper ring"; the lower ring is the "central ring". The dark colored atom on the keeper ring is the main chain oxygen (see text). All hydrogen atoms are considered as part of the atom to which they are attached.

IV. GLD Simulation

A. Model. As shown in section III, the local structure quickly equilibrated to a layered structure with only one close neighbor to each repeat unit within a chain. This suggests that we use a reduced model where the single nearest neighbor ring acts as a "keeper ring". The designation of one of the two rings in the reduced model as a central ring and one as a keeper ring is artificial and done for convenience. In reality both of the rings flip and each of them acts as a gate keeper for the other. The two ring reduced model was checked by rotating the central ring in the full lattice and looking at all of the forces acting upon it. It was found that the forces on the central ring were dominated by the nearest neighbor ring and its bonded main chain oxygen. In addition, the full simulation showed no ring angle correlation with any of the neighboring rings (including those on the same chain). A picture of the resulting reduced model on which we will do the GLD simulation is given in Figure 3.

The phenyl rings were kept rigid, as was the ring oxygen bond for the keeper ring. Hence the only motions which were allowed were ring center of mass motion and ring angle oscillations.

Since the other parts of the lattice are deleted, harmonic effective potentials are needed to keep the rings to their equilibrium position,

$$V_x = {}^1/_2 k_x (x - x_o)^2 \tag{16a}$$

with similar potentials V_y and V_z. (z is taken along the chain axis, x is toward the other ring, and y is taken perpendicular to x and z.) To correlate the motion between the two rings, a harmonic effective potential was also used between the centers of mass of the two rings

$$V_{xx} = {}^1/2 k_{xx} (\Delta x - \Delta x_o)^2 \tag{16b}$$

where Δx is the absolute difference between the x coordinates of the centers of mass of the two rings and Δx_o is the equilibrium value of Δx. Similar effective potentials were used for the y and z coordinates. The last effective potential used was an angular effective potential for each ring with a barrier made up of two pieces with opposite curvature.

$$V_\theta = \begin{cases} {}^1/_2 k_1 \theta^2, & \text{where } -\theta_c < \theta < \theta_c \\ V_o - {}^1/_2 k_2 (\pi/2 - |\theta|)^{2n}, & \text{all other values of } \theta \text{ between } \pm\pi/2 \end{cases} \tag{17}$$

where n is an integer. In eq 17, we are taking the equilibrium average position of the ring as $\theta = 0$ and the pieces of the potential with postive and negative curvature and their first derivatives are matched at the crossover angle, θ_c. The angular effective potential is given modulo π.

In addition, we included the inter-ring Lennard-Jones 6−12 potential between all of the atoms using the same parameters used in the full simulation. We also used exponential memory functions for the ring angle, ring center of mass, and ring−ring degrees of freedom.

Lastly, following a common practice in many-body theory,[27] we used effective masses of the rings for the center of mass motion rather than the true masses. The effective mass is heavier in the z direction (along the chain) than it is in the x and y directions due to the effect of the chain on the motion of the ring.

B. Parameter Fitting. In order to fit the parameters, we used both distribution functions and autocorrelation functions obtained from the full simulation. As an example, the ring angular distribution function is given in Figure 4 and the angular autocorrelation function is given in Figure 5. For the center of mass motion and the ring−ring motion we used similar distribution and autocorrelation functions (in each component) which we are not showing. In addition, in order to obtain the barrier height in the ring angle effective potential, we had to make sure that the π-flip frequency was within the frequency distribution obtained by the NMR measurements of the π-flip frequency. It should be pointed out that to within the accuracy of the simulation the distribution function and

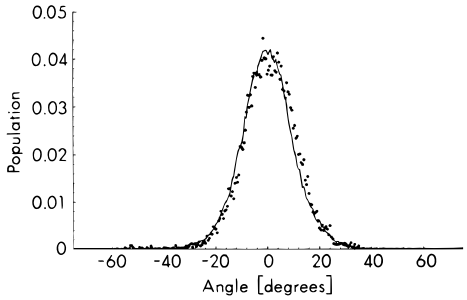

Figure 4. Central ring angular distribution function. The dots are from the full simulation; the solid line is from the GLD simulation.

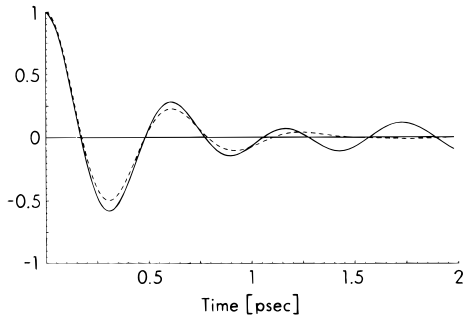

Figure 5. Normalized central ring angular autocorrelation function. The solid line is from the full simulation; the dashed line is from the GLD simulation. Note that the long time oscillation in the autocorrelation function from the full simulation is an artifact, as explained in the text.

autocorrelation function of the central ring and the keeper ring were the same. This showed that the lattice in the full simulation was large enough to eliminate edge effects.

The correlation and autocorrelation function were obtained from a GLD simulation at 300 K, the same temperature as the full simulation. This required only a short GLD simulation. The flip frequency was fit using a high temperature, starting at 900 K (above 900 K the simulation was too noisy to use) and working down in temperature to obtain the flip frequency at 300 K, which we would then compare with experiment. Thus, by working at high temperatures and extrapolating, we did not have to use a long GLD simulation in the fitting procedure. We repeated this procedure until we had a set of parameters that fit all the correlation and autocorrelation functions as well as the experimental π-flip frequency. We then used this set of parameters to work down in temperature to 300 K.

In Figure 4 we have also given the angular correlation function from the GLD simulation as the solid line. It should be noted that we time averaged for 100 ps for the full simulation (the length of the simulation), while for the GLD simulation we time averaged for about 1 ns. Hence all correlation functions obtained from the GLD simulation have better statistics than those obtained from the full simulation. In Figure 5 the dotted line gives the GLD angular autocorrelation function which again has better statistics than the result from the full simulation. The long time oscillating behavior of the autocorrelation function for the full simulation (rather than decaying to zero) is an artifact of low statistics. We obtained autocorrelation functions using a double Fourier transform taking advantage of the Fourier convolution theorem that says that the Fourier transform of a convolution (which an autocorrelation function is) is the product of Fourier transforms. Thus,

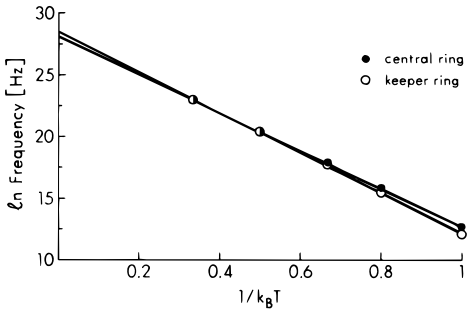

Figure 6. Arrhenius plot for phenyl ring π-flips. The closed (open) circles are for the central ring (keeper ring). The π-flip frequency at 300 K ($k_BT = 1$) is 320 kHz (192 kHz) for the central ring (keeper ring). The π-flip activation energy is 15.4 $k_BT = 38.4$ kJ/mol (16.3 $k_BT = 40.7$ kJ/mol) for the central ring (keeper ring). The experimental π-flip activation energy is 38 kJ/mol.[2]

we averaged the product of the Fourier transform of the angles and back-transformed to get the autocorrelation function. This is much faster than obtaining the autocorrelation function directly. The oscillatory behavior comes from not enough data in the fast Fourier transform steps. The final set of parameters is given in Appendix B.

V. Results from the GLD Simulation

In Figure 6, we give the Arrhenius plot of the natural logarithm of the phenyl ring π-flip frequency vs $(k_BT)^{-1}$ where k_B is in reduced energy units ($1/k_B = 300$ K). The filled circles represent the central ring, while, for comparison, the open circles represent the keeper ring. The frequency of π-flips is one of the fitting parameters, as discussed in section III, so the frequencies of flips obtained from the GLD simulation at 300 K of 320 kHz (192 kHz) for the central ring (keeper ring) is only a consistency check. These frequencies are consistent with the experimental distribution of flip frequencies.[2] However, the activation energy of 38.4 kJ/mol (40.7 kJ/mol) for the central ring (keeper ring) is an independent prediction of the model and is in agreement with the experimental NMR result of Schaefer and co-workers[2] of 38 kJ/mol. As can be seen from Figure 6 the straight line fits to the simulated data is extremely good for both rings. We feel that any statistical analysis of these results would give a much too optimistic view of the precision of these calculations and that a more realistic estimate of the precision is obtained by comparing the results for the two rings. Hutnik *et al.* obtained[13] a value of 43.3 $\pm$ 28.7 kJ/mol for the barrier to phenyl ring π-flips in their energy minimization calculation.

In order to understand the mechanism of phenyl ring π-flips, we must study not only the π-flips themselves but also cases where the rings do not flip. That is, we shall also look at situations where some, but not all, of the conditions for a successful flip (see below) are satisfied, and the ring does not flip. Such failed flips will henceforth be referred to as "flops". In Figures 7−9, we present a series of strip charts of the time course of the relevant parameters obtained for some illustrative examples of both flips and flops obtained from the GLD simulation. Reading from the top of Figure 7, we have the time courses of the central ring angle, the rotational kinetic energy of the central ring, the perpendicular distance between the central ring and the keeper ring, and the angle of the keeper ring. Notice that all of the time courses are the same. Figure 7 shows the only example we saw where a flip was followed closely in

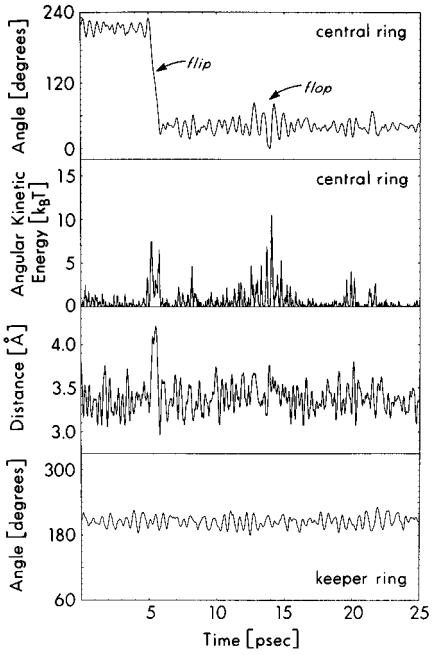

Figure 7. Strip charts showing the time course of the relevant variables for a flip and a flop. The variables depicted are in descending order from the top: the angle of the central ring in degrees, the rotational energy of the central ring in units of k_BT, (1 k_BT = 2.49 kJ/mol), the perpendicular distance between the two rings in Å, and the angle of the keeper ring in degrees. Time is in ps with an arbitrary zero.

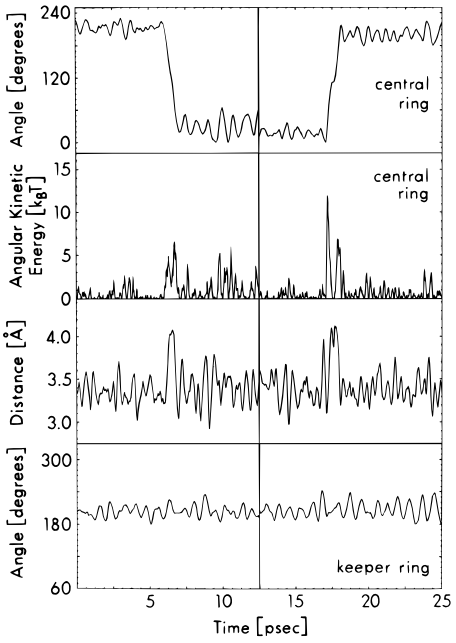

Figure 8. Strip charts showing the time course of the relevant variables for two flips. See legend for Figure 7.

time by a flop. Figures 8 and 9 have joined two separate time panels.

In Figure 7, we see a flip starting at 5 ps. Coincident with the onset of the central ring flip, we see a sharp spike in the rotational kinetic energy of the ring from fluctuations about the equipartition energy of $^1/_2k_BT$ to about 8.5 k_BT (21.2 kJ/mol). At the midpoint of the flip, the kinetic energy drops only to rise again on the downside of the flip. Also coincident with the flip is a sharp increase in the inter-ring distance from one fluctuating around 3.4 Å. This is an increase of 0.5 Å over the largest of the normal fluctuations about the

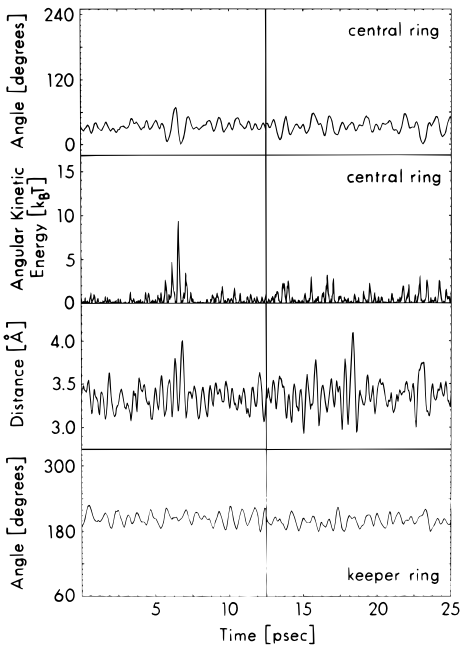

Figure 9. Strip charts showing the time course of the relevant variables for two flops. See legend for Figure 7.

average distance. There is no change in the angular distribution of the keeper ring. It should be noted that while the average time between π-flips is microseconds, the time required for a flip is about 1 ps.

Figure 7 also shows a number of sharp spikes in the angular kinetic energy centered at 14 ps. The largest of these spikes is 10.5 k_BT, which is 4 k_BT (10 kJ/mol) larger than the kinetic energy spike for the previously successful flip. However, there is no coincident change in the inter-ring distance; it continues the normal fluctuation about the equilibrium distance. Hence we observe only an increase in the librational amplitude—a flop.

In the left panel in Figure 8, we again observe a flip with the same characteristic double spike in the rotational kinetic energy as seen in Figure 7, although here somewhat smaller than that in Figure 7. Again this is coincident with a large increase in the inter-chain distance, and the angular distribution for the keeper ring remains normal. In the right panel of Figure 8, we observe another flip with the opposite sense of rotation. This flip is characterized by a slight pause at the midpoint of the flip. Notice that between the double spikes in the kinetic energy the energy has dropped to zero, unlike the situation shown in the left panel, where the kinetic energy has remained positive. There is also a very short duration closing down of the ring distance by a little over 0.2 Å, coincident with this pause at the center of the flip.

In Figure 9, we present two further examples of flops. In the right panel, we observe that there is a large increase in the inter-ring distance to 4.1 Å. This is a large enough distance fluctuation to result in a flip (compare with the left panel of Figure 8) if it were accompanied by a kinetic energy spike—but it is not. Hence we have a flop. In this case, there is not even an increase of librational amplitude, unlike the example shown in Figure 7, where we had an energy spike but no increase in the inter-ring distance.

The left panel of Figure 9 is perhaps the most interesting case of a flop. Here we have a large kinetic energy spike and also a large increase in the inter-ring

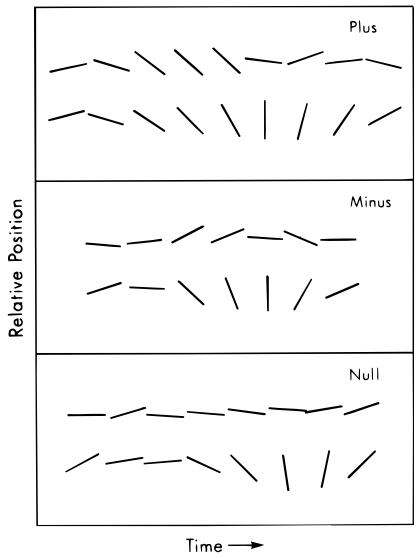

Figure 10. Pictorial time sequence of three flips. The flip axis is coming out of the paper, and time increases left to right. In all three pictures, the keeper ring is the upper ring and the central ring (the flipper) is the lower ring. The plus (minus) denotes that the keeper ring is twisting with the same (opposite) sense of rotation as the flipping ring. The zero is for a case where the keeper ring is not twisting.

separation distance but no flip. A close examination of these two time courses (with the aid of a straight edge) reveals that the kinetic energy spike and the inter-ring separation spikes are out of phase with each other. That is, the increase in the inter-ring separation coincides with a minimum in the kinetic energy rather than with a maximum. Thus, when there is enough kinetic energy for a flip, there is no separation, and when there is a separation, there is no kinetic energy, resulting in a flop with a large librational amplitude.

Figure 10 shows a pictorial time sequence of three flips looking down the chain (*i.e.*, the flip axis is coming out of the paper). In each case, the central ring (the flipper) is the lower ring and the keeper ring is on top and time increases left to right. In the upper panel, denoted plus, the keeper ring librates with the same sense of rotation as the flipper (clockwise) to help reduce the steric barrier. In the middle panel, denoted minus, the keeper ring librates with the opposite sense of rotation to the flipper, which again is rotating clockwise. These plus and minus rotating mechanisms were equally common in the simulations. The lower panel, denoted zero, shows a case where the keeper ring does not librate to help the flipper over the barrier. This zero rotating mechanism was much rarer, occurring only twice for the 51 observed central ring flips (26 at 375 K and 25 at 300 K). Lastly, we never observed the two rings flipping together in a concerted fashion, and we never observed a 2π ring-flip. Such a 2π ring-flip, if it occurred, would be unobservable in the NMR experiments.[2]

VI. Conclusions and Discussion

From the GLD simulation on the reduced model we have seen that a phenyl ring π-flip occurs when (i) there is an increase in the separation distance between a phenyl ring and its nearest neighbor phenyl ring on another chain of between 0.4 and 0.6 Å; (ii) at the same time, there is an increase in the rotational kinetic energy of the flipping ring by about 12−25 kJ/mol; and (iii) the increase of the separation distance and the increase of the rotational kinetic energy must be in phase with each other.

In addition, we also observed that usually, the non-flipping ring twists slightly to help the flipper. There were no double π-flips where two phenyl rings on nearest neighbor chains flipped together in concert. There were no flips of greater than π, *i.e.*, 2π, 3π, etc.

We can understand the condition for phenyl ring π-flips by recalling that in isolated polycarbonate chains (*e.g.*, in solution) the phenyl rings are essentially free rotors. In a solid glass, the phenyl rings are locked in place by the steric repulsion due to a ring on the nearest neighbor chain. When the rings move apart, the steric repulsion barrier to rotation is lowered. In order for the rings to move apart, the chains must flex (since they cannot move apart as stiff units). This flexing requires energy; hence the amount of flex is limited. The extent to which the rings can move apart lowers the steric barrier to flipping but does not remove it. Hence, there must be a kinetic energy fluctuation in the rotational coordinate to enable the ring to go over the residual barrier. This energy fluctuation must occur at the same time the rotational barrier is reduced by the rings moving apart due to the chain flexing. Since both the large flexing action of the chain and the rotational kinetic energy fluctuation are low probability events, the coincidence is a very low probability event, hence the low frequency of phenyl ring π-flips.

The nonoccurrence of (or better, the very low probability of) two adjacent rings flipping together is due to the very low probability that both will have a rotational kinetic energy fluctuation at the same time as their mutual increased separation reduces the rotational barrier for both rings. Since the energy fluctuations are essentially independent events for each ring, the probability that both rings will have the necessary fluctuation within the window of opportunity afforded by the barrier lowering is the square of the probability that one ring will have such a fluctuation and therefore flip.

In a similar vein, the reason we do not see $n\pi$-flips ($n > 1$) is that the time duration of both the increased separation and the energy fluctuation are very short, ca. 1 ps; hence there is very little chance for rotation of greater than π. Or said another way, the hole which allowed the flip closes down very quickly, trapping the ring again by the steric rotation barrier. We can also surmise, from the lack of any angular correlation between neighboring rings on the same chain observed in the full simulation, that the occurrence of coincident π-flips of two neighboring rings on the same chain is also a very low frequency event—although clearly our reduced simulation has nothing to say about such events.

The understanding of the phenyl ring π-flips and the relationship of these flips to the dynamic mechanical loss spectrum allows us the luxury of speculating (in an informed way, we hope) on the unusual toughness properties of polycarbonate. In order to resist failure when struck by a sharp impact, the energy of the impact must be quickly dissipated before the energy can coalesce into a mode which would cause failure. This energy dissipation removes the energy from the region of the impact and eventually reduces it to heat. While failure mechanisms are clearly nonlinear, energy transport and dissipation are in the linear response regime. Linear response implies, via a fluctuation dissipation theorem, that the motions we are studying by thermal fluctuation (phenyl ring π-flips) are the same motions that respond to a perturbation. So we now can ask how this interchain motion which allows the phenyl ring

π-flips serves in the transport of energy. In order to have fast energy transport, there must be a large amount of order in the structure, *i.e.*, a large cooperative unit or bundle—after all, good crystals have high thermal conductivity. In a glassy polymer, this requires a high degree of local order (parallelism) which allows the energy to be transported quickly to the bundle's periphery. Here the weaker thermal contact between the bundles allows for the more orderly intrabundle vibrational motion to be dissipated into frictional interbundle motion, *i.e.*, degraded into heat. In this context, one should note that the −80 °C peak of the dynamic mechanical loss spectrum has been interpreted as being due to interbundle motion.[4]

A more accurate, but less pictorial, way of describing this process is that the flexing mode quickly propagates across the chain, taking advantage of the short range order, *i.e.* parallelization of the chains. As the mode propagates, the direction of local parallelization changes since there is no long range order in the glass. Mostly, this is a gradual, *i.e.* quasi-continuous change, since there is a local order almost everywhere in the glass. Hence, the flexing mode can continue to propagate; however, the propagation direction changes, and over a long distance, randomizes. In addition, as the order changes, the propagation mode has to be continuously projected onto the new direction of propagation. This projection results in a continuous bleeding off of some of the energy of the propagating mode into other vibrational modes as it propagates further from the source. Thus, due to this increasing dispersion of the energy into more and more vibrational modes, the energy is degraded into heat. Of course, there are also local defects, such as bends or kinks, which also serve to disperse the transverse flexing mode. Hence, we have a rapid propagation of energy, due to the local order and transverse flexing mode as well as a rapid degradation into heat due to the absence of a long range order.

As we have previously shown,[11] the degree of local order (parallelism) in polymer chains increases with the increasing stiffness of the chain. However, in order for the chain to be able to flex enough to allow for the interchain motion which gives rise to the phenyl ring π-flips, there must be some flexibility in the chain. Hence, in polycarbonate, there is a compromise between the stiffness necessary to have large cooperative units and the flexibility necessary to allow the large amplitude motion necessary to efficiently transport the impact energy. We suggest that it is just this compromise that gives polycarbonate its unusual toughness properties.

Acknowledgment. The authors thank our colleagues Jake Schaefer, Chris Klug, Ken Tasaki, and the rest of the Schaefer research group (past and present) without whose help and collaboration the present work could not have been done. This work was supported by NSF grant DMR-9015864.

Appendix A. Parameters for the Full Simulation

Table A1. United Atoms

type	symbol	mass (Da)
aromatic carbon	C_A	12
aromatic carbon and hydrogen	CH	13
carbonyl carbon	C	12
quaternary carbon	C_Q	12
methyl group	CH_3	15
ketone oxygen	O	16
carbonyl oxygen	O_C	16

Table A2. Parameters for Potential between Bonding Atoms, Eq 9

type	b_0 (Å)	k_b [kcal/(Å^2 mol)]
CH−CH	1.383	880
CH−C_A	1.383	880
C_A−O	1.4	730
C_A−C_Q	1.52	690
C−O	1.34	700
C−O_C	1.16	1280
C_Q−CH_3	1.53	536

Table A3. Parameters for Bond Angle Potential, Eq 10

type	θ (deg)	k_θ [kcal/(rad^2 mol)]
CH−CH−C_A	120	140
CH−C_A−CH	120	140
CH−C_A−O	116	160
CH−C_A−C_A	122	144
C_A−O−C	117	140
C_A−C_Q−C_A	110.5	140
C_A−C_Q−CH_3	111.6	140
CH_3−C_Q−CH_3	112.7	116.7
O−C−O	111.5	262
O−C−O	122.5	262

Table A4. Parameters for Torsion Angle Potential, Eq 11

type	n	ϕ (rad)	k_ϕ (kcal/mol)
CH−CH−C_A−CH	π	2	2.8
C_A−CH−CH−C_A	π	2	2.8
CH−CH−C_A−O	π	2	3.1
CH−CH−C_A−C_Q	π	2	3.1
CH−C_A−O−C	π	2	0.2
CH−C_A−C_Q−CH_3	0	6	0.01
C_A−O−C−O	π	2	2.5
C_A−O−C−O_C	π	2	2.5

Table A5. Parameters for Improper Torsional Potential, Eq 12

type	ϕ (rad)	$k_{i\phi}$ [kcal/(rad^2 mol)]
CH−C_A−CH−CH	0	30
CH−CH−CH−C_A	0	30
CH−CH−CH−O	0	180
C_A−CH−CH−C_Q	0	274
C−O−O−O_C	0	294

Table A6. Parameters for Special Torsional Potential, Eq 14

type	k_r (kcal)
CH−C_A−C_Q−C_A	0.225

Table A7. Lennard-Jones Parameters, Eq 13[a]

type	σ (Å)	ϵ (kcal/mol)	type	σ (Å)	ϵ (kcal/mol)
C_A	1.77	0.0500	CH_3	1.927	0.1811
CH	1.77	0.0903	O	1.40	0.1591
C	1.67	0.1410	O_C	1.36	0.1591
C_Q	1.60	0.0903			

[a] We use the standard combining rules: arithmetic for σ ($\sigma_{ij} = \sigma_i + \sigma_j$), geometric for ϵ [$\epsilon_{ij} = (\epsilon_i\epsilon_j)^{1/2}$]. Intra-chain σ_{ij}'s are given by $0.89(\sigma_i + \sigma_j)$.

Table A8. Parameters for Constraint Potential, Eq 15

type	s_0 (Å)[a]	k_c [kcal/(Å mol)]	average s (Å)[a]
C−C	6.0	500	5.82 ± 0.21
C−C_Q	5.1	500	5.23/5.16[c] ± 0.14
C−CH_3	4.6	100	4.51/6.14[c] ± 0.17

[a] Experimental value of the distance. The experimental error is ±0.4 for each distance. [b] This is the average for the final simulation at 300 K. The error listed is the half-width at half-maximum of time distance distribution function. [c] The first number is the average for the constrained layer; the second is that for the unconstrained layer, which in the case of the C−CH_3 distance is for a methyl pointing away from the carbonyl carbon. See Figure 2.

Table A9. Simulation Parameters for the Full Simulation

time step (fs)	0.25
relaxation time (ps)	1−2
temp (K)	0−100
equilibration time (ps)	10
temp (K)	300
simulation time (ps)	100
simulation temp (K)	300
sampling frequency (fs)	5
friction coefficient (Å/ps)	1
Lennard-Jones cutoff radius (Å)	9

Appendix B. Simulation Parameters for the GLD Simulation

Table B1. Memory Function Parameters, Eq 8

coordinate	α [kJ/(mol ps)]	γ (ps^{-1})
θ	220.3	55.20
x	550.7	55.20
y	516.3	55.20
z	495.6	55.20

Table B2. Ring Center Potential Parameters, Eq 16a

			potential minimum (Å)	
coordinate	k [kJ/(mol Å^2)]	coordinate	central ring	keeper ring
x	57.37	x_o	−10.38	−13.69
y	81.06	y_o	−15.04	−13.16
z	46.14	z_o	−27.50	−30.26

Table B3. Ring−Ring Potential Parameters, Eq 16b

coordinate	k [kJ/(mol Å^2)]	potential minimum (Å)
x	8.73	2.243
y	33.42	1.765
z	22.82	2.810

Table B4. Ring Angle Potential Parameters, Eq 17

ring	n	θ_c (deg)	V_O (kJ/mol)	k [kJ/(mol rad^2)]
central	2	12.0	5.11	44.90
keeper	1	25.0	18.80	44.90

Table B5. Effective Masses and Moment of Inertia of the Rings

direction	effective mass (g/mol)
x, y	104
z	266
moment of inertia [(g Å^2)/mol)]	
74.60	

References and Notes

(1) Schaefer, J.; Stejskal, E. O.; McKay, R. A.; Dixon, W. T. *Macromolecules* **1984**, *17*, 1479.
(2) Walton, J. H.; Lizak, M. J.; Conradi, M. S.; Gullion, T.; Schaefer, J. *Macromolecules* **1990**, *23*, 416.
(3) Schaefer, J.; Stejskal, E. O.; Buchdahl, R. *Macromolecules* **1977**, *10*, 384.
(4) Lee, P. L.; Kowalewski, T.; Poliks, M. D., Schaefer, J. *Macromolecules* **1995**, *28*, 2476.
(5) Schaefer, J.; Stejskal, E. O.; Perchak, D.; Skolnick, J.; Yaris, R. *Macromolecules* **1985**, *18*, 368.
(6) Perchak, D.; Skolnick, J.; Yaris, R. *Macromolecules* **1987**, *20*, 121.
(7) Romiszowski, P.; Yaris, R. *J. Chem. Phys.* **1991**, *94*, 6751; *95*, 6738.
(8) Klug, C. A.; Zhu, W.; Tasaki, K.; Schaefer, J. *Macromolecules* **1997**, *30*, 1734.
(9) Henrichs, P. M.; Luss, H. R. *Macromolecules* **1988**, *21*, 860. Henrichs, P. M.; Luss, H. R.; Scaringe, R. P. *Macromolecules* **1989**, *22*, 2731.
(10) Altmann, S. L. *Band Theory of Solids: an Introduction From the Point of View of Symmetry;* Clarenden Press, Oxford, U.K., 1991; p 200. Sutton, A. P. *Electronic Structure of Materials;* Clarenden Press, Oxford, U.K., 1993; p 38.
(11) Kolinski, A.; Skolnick, J.; Yaris, R. *Macromolecules* **1986**, *19*, 2250.
(12) Kowalewski, T.; Schaefer, J. Unpublished results.
(13) Hutnik, M.; Argon, A. S.; Suter, U. W. *Macromolecules* **1991**, *24*, 5970.
(14) Hutnik, M.; Gentile, F. T.; Ludovice, P. J.; Suter, U. W.; Argon, A. S. *Macromolecules* **1991**, *24*, 5962.
(15) Langevin, P. *Compt. Rend.* **1908**, *146*, 530.
(16) Zwanzig, R. *Annu. Rev. Phys. Chem.* **1965**, *16*, 67. Mori, H. *Prog. Theor. Phys.* **1965**, *33*, 423. Kubo, R. *Prog. Theor. Phys.* **1965**, *29*, 255.
(17) Abrikosov, A. A.; Gorkov, L. P.; Dyzaloshinski, I. E. *Methods of Quantum Field Theory in Statistical Physics*; Prentice Hall: Englewood Cliffs, NJ, 1961. Csanak, G.; Taylor, H. S.; Yaris, R. *Adv. At. Mol. Phys.* **1971**, *7*, 287.
(18) Smith, D. E.; Harris, C. B. *J. Chem. Phys.* **1990**, *92*, 1304.
(19) *QUANTA: Parameter Handbook*; Molecular Simulations, Inc.: Waltham, MA, 1992.
(20) Hutnik, M.; Argon, A. S.; Suter, U. W. *Macromolecules* **1991**, *24*, 5956.
(21) Kremer, K.; Grest, G. S. *J. Chem. Phys.* **1990**, *92*, 5077.
(22) Allen, M. P.; Tildesley, D. J. *Computer Simulation of Liquids*; Clarendon Press: Oxford, U.K., 1989.
(23) See appendix of ref 6.
(24) Perez, S.; Scaringe, R. P. *Macromolecules* **1987**, *20*, 68. Chu, A. H.; Paul, D. R. *Polym. Eng. Sci.* **1980**, *20*, 87.
(25) Schaefer, J.; Stejskal, E. O.; McKay, R. A.; Dixon, T. W. *Macromolecules* **1984**, *17*, 1479.
(26) Lee, P. L.; Schaefer, J. *Macromolecules* **1995**, *28*, 1921.
(27) See, *e.g.*: Ter Haar, D. *Introduction to the Physics of Many-Body Systems*; Interscience: New York, 1958.

MA9611432